High-throughput enzyme screening platform for the IPP-bypass mevalonate pathway for isopentenol production

Kang, Aram; Meadows, Corey W.; Canu, Nicolas; Keasling, Jay; Lee, Taek Soon

Published in:
Metabolic Engineering

Link to article, DOI:
10.1016/j.ymben.2017.03.010

Publication date:
2017

Document Version
Peer reviewed version

High-throughput enzyme screening platform for the IPP-bypass mevalonate pathway for isopentenol production

Aram Kang[1,2], Corey W. Meadows[1,2], Nicolas Canu[1], Jay D. Keasling[1,2,3,4,5], Taek Soon Lee[1,2,*]

[1]Joint BioEnergy Institute, 5885 Hollis Street, Emeryville, CA 94608, USA.

[2]Biological Systems & Engineering Division, Lawrence Berkeley National Laboratory, Berkeley, CA 94720, USA.

[3]Department of Bioengineering, University of California, Berkeley, CA 94720, USA.

[4]Department of Chemical and Biomolecular Engineering, University of California, Berkeley, CA 94720, USA.

[5]The Novo Nordisk Foundation Center for Biosustainability, Technical University of Denmark, Denmark

[*]Corresponding author: Dr. Taek Soon Lee, Joint BioEnergy Institute, 5885 Hollis St. 4th floor, Emeryville, CA 94608, USA; Phone: +1-510-495-2470, Fax: +1-510-495-2629, E-mail: tslee@lbl.gov

Keywords: Isopentenol, isoprenol, mevalonate pathway, biofuel, phosphomevalonate decarboxylase, enzyme screening

Abstract

Isopentenol (or isoprenol, 3-methyl-3-buten-1-ol) is a drop-in biofuel and a precursor for commodity chemicals such as isoprene. Biological production of isopentenol via the mevalonate pathway has been optimized extensively in *Escherichia coli*, yielding 70% of its theoretical maximum. However, high ATP requirements and isopentenyl diphosphate (IPP) toxicity pose immediate challenges for engineering bacterial strains to overproduce commodities utilizing IPP as an intermediate. To overcome these limitations, we developed an "IPP-bypass" isopentenol pathway using the promiscuous activity of a mevalonate diphosphate decarboxylase (PMD) and demonstrated improved performance under aeration-limited conditions. However, relatively low activity of PMD toward the non-native substrate (mevalonate monophosphate, MVAP) was shown to limit flux through this new pathway. By inhibiting all IPP production from the endogenous non-mevalonate pathway, we developed a high-throughput screening platform that correlated promiscuous PMD activity toward MVAP with cellular growth. Successful identification of mutants that altered PMD activity demonstrated the sensitivity and specificity of the screening platform. Strains with evolved PMD mutants and the novel IPP-bypass pathway increased titers up to 2.4-fold. Further enzymatic characterization of the evolved PMD variants suggested that higher isopentenol titers could be achieved either by altering residues directly interacting with substrate and cofactor or by altering residues on nearby α-helices. These altered residues could facilitate the production of isopentenol by tuning either k_{cat} or K_i of PMD for the non-native substrate. The synergistic modification made on PMD for the IPP-bypass mevalonate pathway is expected to significantly facilitate the industrial scale production of isopentenol.

1 Introduction

Isopentenol (or isoprenol, 3-methyl-3-buten-1-ol) is a promising biofuel and a precursor for industrial chemicals such as isoprene (Beller et al., 2015; George et al., 2015a). The research octane number of isopentenol (98) is close to isooctane (RON = 100), demonstrating its potential use as an anti-knocking additive in gasoline (Liu et al., 2014; Mack et al., 2014). Several microbial hosts have been engineered for biological production of isopentenol with the most commonly targeted pathways including isoprenoid pathways from both the mevalonate (MVA) pathway and the methylerythritol phosphate (MEP) pathway, and the keto acid pathway (Atsumi et al., 2008).

Briefly, the conventional MVA pathway for isopentenol production starts with reactions that condense three acetyl-CoA molecules and produce one molecule of MVA. Next, mevalonate kinase (MK) phosphorylates MVA to mevalonate 5-phosphate (MVAP), which is subsequently phosphorylated to mevalonate 5-diphosphate (MVAPP, also diphosphomevalonate) by 5-phosphomevalonate kinase (PMK). The phosphorylation reactions consume two adenosine triphosphate (ATP) molecules, and then diphosphomevalonate decarboxylase (PMD) converts MVAPP to isopentenyl diphosphate (IPP) while consuming one additional ATP molecule (Figure 1A). Lastly, isopentenol is produced by hydrolysis of the pyrophosphate group from IPP (Chou and Keasling, 2012).

Extensive optimization of the conventional MVA pathway for isopentenol production in *Escherichia coli* resulted in titers of 2.2 g/L with 70% of apparent theoretical yield (George et al., 2014; George et al., 2015b). However, the "IPP-dependency" of the conventional MVA pathway intrinsically limits engineering of the MVA pathway toward high titer isopentenol production for two primary reasons: its high ATP requirement and toxicity of IPP (Kang et al., 2016). First, generation of one molecule of IPP via the MVA pathway requires the consumption of 3 ATP molecules, which accounts for approximately 5.3% of the theoretical ATP yield from complete

aerobic respiration of one and half (1.5) molecules of glucose. However, in the conventional MVA-based isopentenol production pathway, the hydrolysis of the diphosphate group of IPP squanders cellular ATP, underscoring the importance of constructing more energetically efficient pathways for isopentenol production. Secondly, accumulation of IPP has been proposed to inhibit growth of *E. coli* (George et al., 2015b; Kang et al., 2016; Martin et al., 2003). Although specific molecular mechanisms behind the growth inhibition effects of IPP are not clear yet, general stress responses accompanied with the growth inhibition potentially divert carbon flux away from desired isopentenol production (Adolfsen and Brynildsen, 2015; Cohen, 2014; Hengge, 2008; Kang et al., 2016; Sun et al., 2011). Since IPP is an essential precursor for isopentenol production in the MVA pathway, maintaining IPP at the optimal level is critical for efficient isopentenol production while minimizing the growth inhibition by excessive IPP. Therefore, "IPP-dependency" of the MVA pathway makes the engineering of the conventional IPP-dependent MVA pathway for isopentenol production more complicated and inefficient.

To overcome the limitations of the IPP-dependent conventional MVA pathway, an IPP-bypass MVA pathway has been developed (Kang et al., 2016) (Figure 1A). A heterologously expressed *Saccharomyces cerevisiae* PMD enzyme (PMDsc) promiscuously decarboxylates MVAP to form isopentenyl phosphate (IP), which is hydrolyzed to isopentenol by endogenous phosphatases. This novel IPP-bypass MVA pathway significantly reduced IPP toxicity and made isopentenol production more robust relative to the native MVA pathway under aeration-limited conditions by decreasing ATP consumption (Kang et al., 2016). Despite its lower toxicity and higher energetic efficiency, isopentenol production via the IPP-bypass MVA pathway was limited by relatively low activity of PMDsc toward the alternative substrate, MVAP (k_{cat} = 0.14 sec^{-1}) compared to the activity toward MVAPP, the original substrate (k_{cat} = 5.4 sec^{-1}) (Kang et al., 2016; Krepkiy and Miziorko, 2004). Therefore, engineering PMD to be more active toward

MVAP is necessary to relieve the bottleneck and increase isopentenol titers and productivity of the IPP-bypass isopentenol pathway.

With this goal, we developed a growth-linked selection method to screen PMD mutants with improved activity toward MVAP. In this new screening platform, we coupled PMDsc substrate promiscuity to the formation of IPP and dimethylallyl pyrophosphate (DMAPP), essential metabolites for *E. coli* growth. IPP production from the endogenous MEP pathway was eliminated by supplementing an antibiotic that inhibits the MEP pathway. *E. coli* growth was rescued only by co-expression of the heterologous IPP-bypass pathway containing sufficiently active PMDsc to convert MVAP to IP with isopentenyl phosphate kinase (IPK), which produces IPP from IP. Using the growth-linked screening platform, we evaluated libraries of PMD variants and identified mutations that improve isopentenol production in *E. coli* via the IPP-bypass MVA pathway.

2 Results and Discussion

2.1 Design of screening platform and optimization

We designed the screening platform in which the growth rate of the host strain is coupled to the decarboxylation rate of the PMD enzyme (Figure 1B). To link cellular growth rates directly with MVAP decarboxylation rates, IPP produced via the endogenous MEP pathway should be blocked either by gene knock-out or by inhibition. Genes involved in the MEP pathway, however, are essential for *E. coli* growth (Heuston et al., 2012), making development of a knockout mutant difficult. Therefore, we chose the second option that is to inhibit the MEP pathway by the addition of the MEP pathway inhibitor fosmidomycin (Zhang et al., 2011). Fosmidomycin is an antibiotic that inhibits 1-deoxy-D-xylulose 5-phosphate reductoisomerase (DXR) of the MEP pathway in native *E. coli*, and it ultimately blocks the only route to generate IPP and DMAPP. By adding fosmidomycin to the cultures of the screening platform strain, isoprenoids for *E. coli* growth could solely be derived from carbon flux through the heterologously expressed IPP-

bypass MVA pathway in the presence of an adequate enzyme to convert IP to IPP. In nature, archaea have a unique isoprenoid pathway where IP is phosphorylated to IPP by IP kinase (Chen and Poulter, 2010). In our screening platform, archaeal IP kinases (IPK) were heterologously expressed to generate IPP via phosphorylation of IP produced from the IPP-bypass MVA pathway (Figure 1B).

We tested for fosmidomycin sensitivity by introducing various amounts of fosmidomycin into DH1, BW25113 and BL21 (Supplementary Table S1), three *E. coli* strains commonly used for microbial metabolic engineering. DH1 was significantly more susceptible than the other two strains (Supplementary Figure S1) to fosmidomycin, as it was the only strain that had no growth on 10 μM fosmidomycin. At higher concentrations of fosmidomycin, cell death was accelerated in DH1, supported by a fast reduction in optical density (OD) at 600 nm after approximately two hours of exposure to fosmidomycin. On the other hand, both BL21 and BW25113 continued to grow for approximately four hours when exposed to equivalent fosmidomycin levels (Supplementary Figure S1). Therefore, DH1 was selected as a host strain to screen PMD mutants for improved MVAP decarboxylation activity and subsequent isopentenol production in this study.

We subsequently confirmed that growth inhibited by fosmidomycin resumed in DH1 by allowing IPP production from IP, which is generated via the IPP-bypass MVA pathway (Figure 1). Three kinases with previously reported activity towards IP—IspE from *E. coli* (EcIPK) (Lange and Croteau, 1999) and two archaeal IP kinases (Funke et al., 2010) from *Methanothermobacter thermautotrophicus* (MtIPK) and *Thermoplasma acidophilum* (TaIPK) — were heterologously expressed (JBEI-15323, JBEI-15642 and JBEI-15350, respectively) in DH1 together with wild type PMDsc (JBEI-15645). Expression of two archaeal IP kinases, MtIPK, and TaIPK, enabled growth recovery of the DH1 strains under fosmidomycin selection pressure, suggesting higher kinase activity of MtIPK and TaIPK compared to that of EcIPK (Figure 2A).

Between two strains expressing the archaeal IPKs, the strain that expressed the MtIPK showed a shorter lag phase (2 hours vs 3-4 hours) regardless of expression level of PMDsc (10 or 100 nM anhydrotetracycline (aTc)) (Lee et al., 2011), suggesting that MtIPK provides better sensitivity to the screening platform. On the other hand, when an inactive mutant, PMDsc-S208E (Kang et al., 2016), was co-expressed (JBEI-15647), none of three IPK-expressing DH1 strains (SP4, SP5 and SP6, Supplementary Table S1) could grow. This result supports our screening platform design hypothesis, which implies that cellular growth is solely dependent upon decarboxylation of MVAP within the heterologously expressed IPP-bypass pathway. In addition, resistance to fosmidomycin, which could be developed by adaptive mutations (Martinez and Baquero, 2000), was not observed under the condition of the screening platform and during growth recovery experiments.

After optimizing the screening conditions where *E. coli* DH1 can survive only from IPP produced from IP generated solely from the MVA pathway, we tested whether the growth rate of *E. coli* DH1 correlated with the relative enzyme activity of PMDsc on MVAP. The kinetics of six PMDsc variants (K22M, R74H, I145F, T209D, S155E and S208E) revealed that two mutants, K22M and R74H, were shown to either decrease or increase isopentenol titers, respectively, in accordance with altering k_{cat} or k_{cat}/K_M of PMDsc for MVAP (Kang et al., 2016). Therefore, the growth rates of K22M and R74H mutants were determined along with positive (WT PMDsc) and negative (inactive S208E mutant) controls under the screening conditions.

As shown in Figure 2b and Supplementary Figure S2, the growth rates of these four strains varied depending on the MVAP decarboxylation activity and expression level of PMDsc. When these enzyme variants were expressed at lower inducer concentrations (10 nM aTc; Supplementary Figure S2a) or with low copy number plasmids (Figure 2b), the growth rates of the DH1 strains harboring the corresponding screening plasmids were dependent on the MVAP-decarboxylation activity of PMDsc variants. Strains with R74H grew faster than the strain with

WT PMDsc, while strain harboring the K22M mutant exhibited decreased growth rates relative to wild type. In addition, it was confirmed that a strain harboring wild type PMDsc grew at different rates when the PMDsc was expressed at different inducer concentrations (data not shown). However, when protein expression levels of PMD variants were increased by using 10-fold higher inducer concentrations (100 nM aTc), all *E. coli* DH1 with active PMDsc variants K22M, R74H, and WT showed similar growth rates ($0.83 \pm .01$ hr^{-1}) (Supplementary Figure S2). This result suggests that expression of PMD needs to be tightly regulated to keep the sensitivity of the screening platform such that the selection pressure would reflect the relative catalytic activity of PMDsc mutants.

Subsequently, the sensitivity and selectivity of the screening platform was further verified by competitive growth among the three DH1 strains containing PMDsc WT, K22M and R74H. A mixed seed culture was prepared by combining an equal starting amount of each of the three strains and incubated overnight. The mixed population was diluted and regrown in fresh medium supplemented with 10 μM fosmidomycin. Sequencing data revealed that DH1 expressing PMDsc-R74H was the dominant strain present after several dilutions of the mixed culture (Supplementary Figure S3). Again, this result confirmed that the screening platform selects for PMDsc mutants with increased activity among a mixed population of strains via growth competition.

2.2 Screening of saturation mutagenesis libraries

After testing selectivity of the screening platform, we constructed and tested two sets of libraries of PMDsc mutants: one library was constructed by codon saturation mutagenesis on seven rationally targeted residues and the other was constructed by error-prone PCR to generate random mutations in PMDsc.

Five residues (Tyr19, Lys22, Ser208, Thr209 and Met212) were selected for codon saturation mutagenesis (Figure 3a). Although a crystal structure of PMDsc with a substrate analog

194 is not available, structural alignment of PMDsc (1FI4) (Bonanno et al., 2001) with a homologous
195 PMD isolated from *Staphylococcus epidermidis* (PMDse) revealed several parallels between their
196 active sites (Barta et al., 2011). Tyr19 and Lys22 in PMDsc correspond to Tyr18 and Lys21 in
197 PMDse, and these homologous residues most likely interact with the pyrophosphate group of the
198 native substrate, MVAPP. The hydroxyl side chain of Ser208 in PMDsc (Ser192 in PMDse) is
199 appropriately positioned to form hydrogen bonds with the α-phosphate moieties of bound ATP
200 and MVAPP in the ternary complex model of PMDse (Barta et al., 2012). Thr209 and Met212 of
201 PMDsc, which correspond to Arg193 and Met196 in PMDse, provide second-sphere structural
202 support for the residues directly interacting with active site substrates (Figure 3a). Two additional
203 residues, Arg74 and Ile145, were also selected based on the previous kinetic data implicating
204 their potential to increase the decarboxylase activity of PMDsc (Kang et al., 2016). R74H and
205 I145F increased k_{cat} for decarboxylation of multiple substrates in PMDsc, including 3-hydroxy-3-
206 methylbutyrate (Gogerty and Bobik, 2010) and MVAP (Kang et al., 2016).
207 Screening of the codon saturation mutagenesis libraries resulted in a dominant amino acid
208 for each residue of Arg74, Ile145, Ser208 and Met212, but the selective effects on the other three
209 residues, Tyr19, Lys22 and Thr209 were not clear and the sequencing result still showed mixed
210 signals of all nucleotides. Three of the four dominant residues, Arg74, Ile145 and Met212, were
211 substituted to serine, alanine and methionine respectively, and we found that these three
212 mutations (M212Q, R74S, and I145A) significantly improved isopentenol production via the IPP-
213 bypass MVA pathway (Figure 3b). DH1 strains expressing these three mutants significantly
214 increased isopentenol production relative to WT (475.1 mg/L), with titers ranging from 600-800
215 mg/L. Such improvement is in line with increases found in R74H (770.3 mg/L) from our previous
216 study (Kang et al., 2016). Interestingly, combinations of select double mutants, R74S-I145A,
217 R74S-M212Q, and R74H-M212Q, significantly increased isopentenol titers by up to 2.4-fold
218 relative to wild type: strains containing these double mutants further improved titers from 900-

1130 mg/L 48 hours after induction with IPTG (Figure 4). Selection of seven codon saturation mutagenesis libraries successfully demonstrated that the screening platform could identify PMDsc mutants that have potentially higher activity towards MVAP and increased isopentenol titers from the IPP-bypass MVA pathway.

In addition to finding mutated residues improving isopentenol production in the IPP-bypass pathway, it also confirmed that the screening platform effectively inhibits the growth of the strain with inactive PMD variants. Alignment-based structural predictions mapping PMDsc to a crystal structure of PMDse suggest that Ser208 forms essential hydrogen bonds with both the α-phosphate of ATP and the α-phosphate of MVAPP. We showed that S208E is inactive toward MVAP (Kang et al., 2016), and another study reported that S208A compromised the structural stability of the PMDsc, resulting in protein precipitation (Krepkiy and Miziorko, 2005). Therefore, viable isopentenol-producing strains retaining the wild-type serine at residue 208 in PMDsc ensured the selection specificity of the screening platform for active PMD sequences. In addition to the S208E mutant, we tested another strain harboring an inactive mutant (S155E) of PMD as a second negative control and reconfirmed the impaired growth phenotype (data not shown). This further supported the wild type selection result of S208 in the saturation mutagenesis library. Hence, strain selection is based solely on the enhancement of carbon flux through the IPP-bypass pathway facilitated by PMDsc activity toward the nonnative MVAP under the screening conditions.

In contrast, Thr209 could be substituted with any amino acid residue (Supplementary Figure S5), suggesting that there was much less selection pressure on this residue within this screening platform. Thr209 of PMDsc is a structurally parallel residue to Arg193 of PMDse, which has been suggested to stabilize the β-phosphate of MVAPP (Barta et al., 2012). Although it was initially hypothesized that this residue might be critical to determine substrate promiscuity, it seems that the decarboxylation activity of PMDsc for MVAP was not significantly affected by

alterations at residue 209. In accordance with this observation, we have shown that T209D did not significantly change the isopentenol titer in *E. coli* (Kang et al., 2016).

2.3 Screening of random mutagenesis libraries

Since the size of the saturation mutagenesis libraries was relatively small (7 x 21 = 147 designs), libraries of randomly mutated PMDsc sequences were prepared by error-prone PCR (McCullum et al., 2010) to contain low-, mid- and high-mutation rates per coding sequence. The DH1 strains carrying JBEI-15350 (Supplementary Table S1) and plasmids libraries of randomly mutated PMDsc were serially diluted into fresh medium containing fosmidomycin to enrich fast-growing strains until the growth rate did not significantly vary among all libraries. In total, there were three rounds of dilutions, but the exposure period of each library to fosmidomycin before the next round of dilution varied depending on the rate of growth recovery. Given the higher heterogeneity of initial libraries, the first dilution significantly extended the lag phase during growth. Thus, all surviving variants after the first selection were rescued overnight in fresh EZ-rich medium without fosmidomycin before the second dilution. At the end of the third dilution, all libraries exhibited similar growth rates (0.72 ±0.10 h^{-1}), which were higher than the average growth rate of the second round (0.49 ±0.11 h^{-1}) and comparable to that of R74H (0.68 ± 0.04 h^{-1}). Sequencing of the amplified PMD sequences revealed that two-thirds of tested libraries were dominated by select PMDsc residues (Table 1), while the remaining mutants were enriched with the wild type PMDsc. Excluding redundant mutations, six unique PMDsc variants were cloned into pTrc99a vector, which were in turn co-transformed with JBEI-9310 (Supplementary Table S1) into DH1 for isopentenol production via the IPP-bypass pathway. Most isopentenol producing strains with respective PMDsc mutants produced isopentenol at higher titers relative to wild type PMDsc except V230E. The highest 48-hour post-induction titers were obtained by the strains with three double mutants, R74G-R147K, Q140L-I226V, and R74G-E144D (Figure 4), whose titers after 48 hours were 1.9-fold, 1.6-fold, and 1.6-fold higher than the strain with wild

type PMDsc, respectively. However, not all selected mutations were cooperative for isopentenol production. R74G and Q140L produced isopentenol at levels similar to or better than those selected from the randomly mutated libraries, R74G-R147K, Q140L-I226Vand R74G-E144D mutants.

2.4 Correlating screening properties to PMD catalytic activity

The rationale behind the screening platform posits that *in vivo* MVAP-decarboxylation activity of PMD in DH1 correlates with the cellular growth rate under conditions where the endogenous MEP pathway is inhibited by fosmidomycin (Figure 1B). This hypothesis assumes that the IPP production rate is limited by MVAP-decarboxylation by PMD (Figure 1A). Isoprenoids are essential for *E. coli* growth. Therefore, MVAP-decarboxylation activity, which is determined by the turnover rate of MVAP to IP *in vivo*, would partially determine the growth rate of a host strain where PMD variants with varying MVAP-decarboxylation activities are expressed in the screening platform (Figure 1B). To further support this hypothesis, we determined the growth rate for twenty mutants that we found in this study under the conditions implemented for mutant screening. The 20 mutants selected for this analysis were representative of all strains producing isopentenol via the IPP-bypass route, ranging from 22 ± 8 mg/L (K22Y) to 1,080 ± 30 mg/L (R74H-R147K-M212Q) (Table 2). As seen in Figure 6, a scatter plot relating cellular growth rates to isopentenol titers shows a positive linear correlation with $R^2 = 0.72$, further corroborating that MVAP decarboxylation is indeed the rate-limiting step in the engineered IPP-bypass pathway. Given that only 20 mutants were identified in the screening platform, a rather low R^2 value was inevitably obtained. However, it should be noted that the correlation between growth rate and isopentenol titers is much better for the eight high-producers of isopentenol (the eight variants at the top right corner), relative to WT (475.1 mg/L and 0.4 h^{-1}, respectively). Although the wider variation in growth rates was observed for poorly producing strains (e.g. two variants at left-bottom corner), it is likely that inactive and less active mutants are more subject to

294 a growth-inhibited phenotype than for more active mutant primed for growth. While the growth
295 phenotype and isopentenol formation are both IP-dependent, variations in growth rates are
296 possible without knowing the kinetic effects of varying IP levels on the growth phenotype within
297 strains used for the screening platform. For this reason, we have noticed that several mutants,
298 particularly with R74S, showed a wider variation in isopentenol titers, possibly due to colony-to-
299 colony variation often observed in over-producing strains. However, these variations found in
300 growth rates and titers do not compromise the validity of the screen design, which demonstrates
301 its selectivity for high-producers over low-producers.

302 **2.5 Potential secondary structure effects of the mutated residues**

303 It is noteworthy that this study identified important residues distal to the active site that
304 enhanced isopentenol production, implicating the possibility that interactions between α-helices
305 could affect the activity of PMDsc for MVAP decarboxylation (Figure 5). The screening platform
306 revealed that two of these helical residues, Arg74 and Ile145, could tolerate several substitutions
307 to facilitate enhanced isopentenol production. In addition to the initially reported mutant (R74H),
308 we found that smaller glycine and serine substitutions were beneficial at position 74, showing that
309 protonated side chains in this locale are not necessary for improving enzymatic activity. While
310 I145F was shown to modestly improve enzyme activity in our previous study (Kang et al 2015),
311 the emergence of I145A from our screening platform showed that packing properties around
312 position 145 can affect the PMDsc activity toward nonnative substrates. However, it is not clear
313 how these distal residues increase activity of PMD toward MVAP. Since both Arg74 and Ile145
314 residues are quite far from the active site (Figure 3a), substitutions at these locales could result in
315 altered interactions between neighboring α-helices. These altered packing modes might cause
316 alternative kinetic consequences rather than directly impacting substrate binding. Particularly,
317 Arg74 appears to shield the active site from bulk solvent by interacting with a loop containing

several substrate binding domain residues (17-33) proposed to be critical for catalysis (Supplementary Figure S4).

The kinetic impact arising from Ile145 is much less clear, as this residue is more than 15 Å away from the cofactor moiety. Interestingly, we found three additional single mutants (Q140L, E144D, R147K) that reside near Ile145, and all of them resulted in increased isopentenol production titers (Figure 4). Gln140, Glu144, Arg147, and Ile145, are all located on α-helix 2 (H2) (Figure 5), and small conformational changes made by these mutants might affect the two serine residues (Ser120 and Ser121) at C-terminal end of H2. These serine residues provide essential hydrogen bonds that stabilize MVAP with ATP (Supplementary Figure S6). In addition to these four residues, we also identified three more distant residues, Gln210, Ile226, and Val230, located on α-helix 4 (H4) (Figure 5), which could alter substrate binding modes for MVAP.

Since we found a positive correlation between isopentenol titers using mutant PMDs and their respective growth rates in the screening platform, we initially expected to see a direct correlation between kinetic parameters (k_{cat} and k_{cat}/K_M) of mutant PMDs and either isopentenol titers or growth rates. However, there was no significant correlation between kinetic activity of mutants and isopentenol and/or cellular growth rates (Supplementary Figure S7). The kinetics of fourteen PMDsc variants for enzymatic decarboxylation (Table 2) showed that many mutants significantly increased k_{cat}/K_M for MVAP, which includes kinetic steps associated with substrate and cofactor binding. However, increasing k_{cat}/K_M does not improve growth rates or isopentenol titers.

The most striking data for k_{cat}/K_M arise from the Y19H and M212Q mutants, which are proposed to interact with the phosphate moieties of the native MVAPP substrate (Figure 3a). Like other diphosphate decarboxylases, the conserved P-loop motif (Barta et al., 2012; Saraste et al., 1990) closes upon ATP binding, which then coordinates substrate and cofactor for catalysis (Barta et al., 2012). Since MVAP lacks the β-phosphate group, the active site needs to be more

compact to prevent packing defects within the active site. In the structural alignment model, the Met212 residue is less than 4 Å from the predicted binding site of the α-phosphate moiety in MVAP (Figure 3a). Therefore, its mutation to glutamine (M212Q) could provide additional hydrogen-bonding interactions with this phosphate moiety to help stabilize MVAP, thereby increasing k_{cat}/K_M (0.5 ± 0.1 mM^{-1} s^{-1}) (Table 2).

Similarly, we hypothesized that mutations at residue 19 might improve stabilization of α-phosphate based on the previous computational study (Weerasinghe and Samantha Dassanayake, 2010), and therefore we aimed to find a better-positioned residue that might interact with the α-phosphate of MVAP. Indeed, Y19H increased k_{cat}/K_M of PMDsc about 10-fold (0.78 ± 0.06 mM^{-1} s^{-1}) (Table 2) compared to that of wild type, exhibiting the largest increase of k_{cat}/K_M relative to wild type. Although both M212Q and Y19H increased k_{cat}/K_M of PMDsc, interestingly only M212Q could significantly increase isopentenol titer, while Y19H rather significantly decreased isopentenol titers (Table 2).

Analysis of all characterized mutants revealed that there was no significant correlation between k_{cat} (or k_{cat}/K_M) and the cellular growth rate or the isopentenol titer (Supplementary Figure S7). For example, the activity of a triple mutant, R74G-R147K-M212Q ($k_{cat}/K_M = 0.5 \pm 0.2$ mM^{-1} s^{-1}), was comparable to that of R74H-R147K-M212Q ($k_{cat}/K_M = 0.4 \pm 0.1$ mM^{-1} s^{-1}), but its isopentenol titer after 48 hours (8 ± 1 mg/L) was 135-fold less than that of R74H-R147K-M212Q (1,079 mg/L). Similarly, R74G's k_{cat}/K_M is comparable to WT's k_{cat}/K_M, but the strain expressing R74G produced significantly higher amount of isopentenol compared to that of WT (Table 2).

2.6 Effect of MVAP inhibition on PMDsc mutants for decarboxylation

The correlation analysis between isopentenol titers and kinetics of the mutants suggested that there must be other factors that determine the actual decarboxylation activity *in vivo* under isopentenol production conditions or growth-based selection conditions. In our previous study,

we found that the *E. coli* production strain containing the IPP-bypass MVA pathway and wild type PMD accumulated significantly higher concentrations of MVAP compared to that of the original pathway within 5 hours after induction (Kang et al., 2016). Assuming *in vivo* MVAP concentrations are well above the K_M (i.e., 10x K_M) for wild type PMDsc (K_M(MVAP) = 2.3 ± 0.2 mM), we hypothesized that noncompetitive substrate inhibition might affect the *in vivo* decarboxylation activity. At such high concentrations of MVAP *in vivo*, the rate enhancements on k_{cat}/K_M or k_{cat} observed *in vitro* for select mutants would not necessarily be observed. Considering the importance of the native mevalonate pathways for isoprenoid metabolism, the activity of PMDsc might be tightly regulated by MVAP concentrations *in vivo* since a low K_I would significantly decrease the rate of decarboxylation as excess MVAP accumulates. This directs MVAP flux through the phosphomevalonate kinase (PMK) enzyme to generate MVAPP, the preferred native substrate for PMDsc, rather than increasing futile decarboxylation of MVAP to IP.

WT and four mutants, R74G, V230E, R74G-R147K-M212Q and R74H-R147K-M212Q, were specifically selected for substrate inhibition study, where activity was measured in wide range of MVAP concentrations up to 100 mM (Figure 7). These variants representatively spanned a wide range of isopentenol titers (8 – 1,080 mg/L), and their substrate inhibition behavior was characterized by determining each mutant's K_I (Table 3). Interestingly, two higher isopentenol producing mutants (R74G and R74H-R147K-M212Q) exhibited significantly higher K_I's (110 mM and 80 mM, respectively) than those with lower isopentenol producers (WT, 18 mM; V230E, 10 mM; and R74G-R147K-M212Q, 11 mM) (Figure 7). A correlation emerged between growth rates (and/or titers) and PMD activity when an observed turnover number was calculated at 100 mM MVAP using the analytical expression for noncompetitive substrate inhibition, k_{obs} (Supplementary Figure S7). This turnover number (k_{obs}) depends upon each mutant's k_{cat}, K_M, and K_I, perhaps yielding a more accurate assessment of the turnover conditions *in vivo* (Kang et al.,

2016). The relationship between growth and k_{obs} of these mutants suggests that the screening platform directly reports on the extent of substrate inhibition in PMDsc mutants (Figure 7 and Supplementary Figure S7). This sensitivity of an *in vivo* screening platform to a mutant's K_I modulation speaks to its power in analyzing the robustness of heterologously expressed mevalonate pathways within overexpressing bacterial strains.

3 Conclusion

Evaluation of enzyme libraries is often limited by the throughput of a screening method. In this regard, growth-based selection is powerful because it does not require extensive tests of an individual design, and designs with the desirable activity are enriched if the activity is essential for growth of the organism (Packer and Liu, 2015). In this study, we designed a growth-based screening platform to improve PMD decarboxylation activity toward MVAP for isopentenol production. To achieve this goal, the growth rate of the *E. coli* DH1 was coupled to the decarboxylation rate of MVAP (Figure 1B); the subsequent product formation of IP is ultimately converted to isopentenol via IPP-bypass MVA pathway (Figure 1A). Codon saturation mutagenesis and random mutagenesis generated two separate enzyme mutant libraries, both of which were tested by our newly developed screening platform. This growth-based screening platform identified a new set of PMDsc mutants that significantly increased isopentenol production up to 1,130±5 mg/L. Correlation of growth rates and decarboxylation rates of identified PMD mutants confirmed the *in vivo* selectivity of the screening platform, and kinetics studies of the mutants suggested the robustness of this screening platform by providing biological context with respect to the target enzyme activity under relevant metabolite concentrations. Alteration of PMD and IPK expression levels coupled with tuning the inhibition strength of fosmidomycin provides the screening platform with more flexibility, potentially enabling further improvements of isopentenol production via the novel IPP-bypass pathway.

4 Materials and Methods

4.1 Plasmids and Strains

All plasmids and strains used in this study are listed in Supplementary Table S1. Primers used for construction of libraries and PMD variants are shown in Supplementary Table S2.

4.2 Development of the PMD screening platform

For the screening platform, a plasmid harboring 6 genes—AtoB, HMGR, HMGS, MK, Idi and a gene coding IP kinase (IPK)—was constructed by adding Idi and IPK to the plasmid (JBEI-9310) used for isopentenol production. AtoB and idi were native genes of *E. coli* while HMGR, HMGS, and MK were derived from *S. cerevisiae*. Two archaeal IP kinases from *Methanothermobacter thermautotrophicus* (MTH) and *Thermoplasma acidophilum* (THA) were amplified from two plasmids, pET15b-MTH and pET28b-THA, respectively (Funke et al., 2010), using primers IPKMTH-F-BglII, IPKMTH-R-XhoI, IPKTHA-F-BglII and IPKTHA-F-XhoI (Supplementary Table S2). A gene coding a potential IP kinase from *E. coli* (EcIPK) was amplified by using two primers EcIPK-BglII-F and EcIPK-XhoI-R (Supplementary Table S2). Wild type PMDsc and PMDsc mutants were cloned into a SC101-based plasmid under control of an araBAD promoter (P_{BAD}) or into a ColE1-based plasmid under control of a Tet promoter (P_{Tet}) (pBbE2a) (Lee et al., 2011). Mutant libraries were transformed in DH1 containing pBbA5c-MevTo-BBa1002-pTrc-MKco-EcIdi-MtIPK (JBEI-15350), and DH1 strains with libraries of PMDsc mutants were tested in the presence of fosmidomycin.

4.3 Cloning and library construction

Seven amino acid residues (Tyr19, Lys22, Arg74, Ile145, Ser208, Thr209, Met212) were selected for saturated mutagenesis. Tyr19, Lys22, Ser208, Thr209, and Met212 were chosen based on their vicinity to the β-phosphate group of MVAPP in a resolved crystal structure of PMDse (Barta et al., 2012) in a structural alignment of PMDsc to PMDse. Additionally, two distal residues, Arg74 and Ile145, have been shown to promote promiscuous decarboxylation activity of PMDsc toward non-native substrates (MVAP and 3-hydroxy-3-methylbutyrate (3-

443 HMB) (Gogerty and Bobik, 2010; Kang et al., 2016). Sequences of primers used for codon
444 saturation libraries are presented in Supplementary Table S2, and amplified PCR products
445 containing specific saturation mutagenesis were cloned to pBbS8a vectors.

446 Randomly mutated PMDsc sequences were generated by error-prone PCR (McCullum et
447 al., 2010) using two primers, j5_00001_(PMDsc)_forward and j5_00002_(PMDsc)_reverse
448 (Supplementary Table S2). The error-prone PCR buffer was supplemented with various
449 concentrations of $MgCl_2$ and $MnCl_2$ to generate different mutation rates. Initially, 100 ng of
450 JBEI-12052 (Supplementary Table S1) was used as a template for PCR, and 1 μL Taq
451 polymerase and 1 μL of 50 mM $MnCl_2$ (final 0.5 mM) were added just before the PCR runs.
452 Every 5 cycles, PCR product was diluted 10-fold in fresh error-prone PCR buffer and additional 1
453 μL Taq polymerase and 1 μL 50 mM $MnCl_2$ (Final would be 0.5 mM) was added to 100 μL PCR
454 reactions. To prepare low-mutation-rate libraries, a few PCR reactions were prepared with lower
455 concentration of $MnCl_2$ and/or $MgCl_2$ with only 5 cycles. All PCR products were digested with
456 DpnI to remove the template plasmids. Purified PCR products were assembled into pBbE2a by
457 Gibson assembly.

458 Randomly mutated PMDsc sequences were grouped into three libraries according to their
459 mutation rates, low (1-2 bases per coding sequence (CDS)), mid (3-4 bases per CDS) and high
460 (more than 10 bases per CDS) mutation rates. These three libraries were transformed in the
461 screening host strain DH1 and three colony-full plates were used for the screening. Number of
462 colonies on each plate was estimated to around 10^3-10^4.

463 **4.4 Screening procedures and conditions**

464 Saturation mutagenesis libraries of PMDsc cloned into a SC101-based plasmid under
465 control of an araBAD promoter (P_{BAD}) were transformed into in *E. coli* DH1 strains harboring
466 JBEI-15350 (Supplementary Table S1). Cultures were suspended in EZ-Rich medium containing
467 1 % glucose, 0.1 mM IPTG, 30 μg/mL chloramphenicol (Cm) and 100 μg/mL ampicillin (Amp),

and incubated at 37 °C at 200 rpm overnight. These cultures were diluted to OD 0.3 in 500 μL EZ-rich medium containing 1 % glucose, 0.1mM IPTG, 50 μM fosmidomycin, and 10mM arabinose. 500 μL cell cultures were prepared in 96 deep-well plates and incubated at 37°C with a shaking speed of 700 rpm in a rotary shaking incubator (HT Infors Multitron; 44% humidity). After 16-18 hours of incubation (Day 2), the overnight cultures were diluted again to OD 0.1 in fresh 500 μL EZ-rich medium containing 1 % glucose, 0.1 mM IPTG, 50 μM fosmidomycin and 10mM arabinose. 500 μL cell cultures were prepared in 96 deep-well plates incubated at 37°C and a shaking speed of 700 rpm in a rotary shaking incubator (HT Infors multitron; 700 rpm, 37°C, 44 % humidity) for 8-16 hours. Next day (Day 3), the overnight cultures were diluted to initial OD of 0.05 in 200 μL EZ-rich medium containing 1 % glucose, 0.1mM IPTG, 50 μM fosmidomycin and 10mM arabinose, and the optical density at 600 nm were obtained in the 96-well plates incubated at 37°C at a shaking speed of 173 rpm (linear, 1 amplitude) in a Tecan F200Pro microplate reader (Tecan, USA).

Random mutagenesis library of PMDsc was cloned into a ColE1-based plasmid under control of a Tet promoter (P_{Tet}) and transformed into *E. coli* DH1 strains harboring pBbA5c-MevTo-BBa1002-pTrc-MKco-EcIdi-MtIPK (JBEI-15350, Supplementary Table S1). DH1 strains with the random mutagenesis library were re-suspended and diluted to OD 0.2 in 100 μL of EZ-Rich medium containing 1 % glucose, 0.1 mM IPTG, 30 μg/mL Cm, and 100 μg/mL Amp, 50 μM fosmidomycin, and 100 nM anhydrotetracycline (aTc). Cell cultures were prepared in 96-well plates (Nunc) and incubated at 37 °C with shaking speed of 173 rpm (linear, 1 amplitude) in a Tecan F200Pro microplate reader (Tecan, USA). After 24 hours of incubation (Day 2), the overnight cultures were diluted 100-fold in 2 mL EZ-rich medium containing 1 % glucose, to recover surviving strains. The overnight cultures were challenged again by diluting them to OD 0.05 in 100 μL EZ-rich medium containing 1 % glucose, 0.1 mM IPTG, 50 μM fosmidomycin, and 10 nM aTc. The 96-well plates were incubated at 37°C at a shaking speed of 173 rpm (linear,

493 1 amplitude) in a Tecan F200Pro microplate reader (Tecan, USA), and cell cultures were
494 subsequently diluted to OD 0.05 once growth reached the exponential phase. The dilutions were
495 continued until the growth rate of all libraries reached that of R74H.

496 **4.5 Isopentenol production in *E. coli***

497 For isopentenol production, *E. coli* DH1 was transformed with two plasmids (JBEI-9310
498 and pTrc99a plasmids expression PMDsc variants; Supplementary Table S1), and isopentenol
499 production was performed as previously described (Kang et al., 2016). Briefly, seed cultures were
500 prepared from single colonies, grown overnight and diluted to OD 0.05 in EZ-Rich defined
501 medium (Teknova, USA) containing 10 g/L glucose (1 %, w/v), 100 μg/mL ampicillin, and 30
502 μg/mL chloramphenicol. Cell cultures (5 mL) were grown at 37°C at a shaking speed of 200 rpm.
503 At OD_{600} of 0.4-0.6, 0.5 mM IPTG was added to the cell cultures to induce expression of genes
504 from the two plasmids, and the cultures were incubated at 30°C and 200 rpm for up to 48 hours.
505 For isopentenol quantitation, an aliquot of cell cultures (270 μL) was combined with 270 μL ethyl
506 acetate containing 1-butanol (30 mg/L) as an internal standard, and the mixture were vigorously
507 mixed for 15 min to extract isopentenol in the cell culture to the ethyl acetate. After extraction,
508 cells were centrifuged at 20,000 x g for 2 minutes, and 100 μL of the ethyl acetate layer was
509 diluted 5-fold in ethyl acetate containing 1-butanol (30 mg/L). An aliquot (1 μL) of each of the
510 diluted samples was analyzed by Thermo GC-FID equipped with DB-WAX column (Agilent,
511 USA).

512 **4.6 Protein expression and purification**

513 Protein expression and purification protocols were performed in a manner similar
514 previously published with minor modifications (Kang et al., 2016). Namely, PMDsc mutant
515 plasmids were harbored in the Rosetta (DE3) bacterial strain as opposed to the BL21(DE3) strain
516 (Supplementary Table S1). Seed cultures were grown and harvested in Terrific Broth medium
517 with 2% glycerol containing 50 mg/L kanamycin and 30 mg/L chloramphenicol. Cells were

initially grown at 37°C with shaking at 200 rpm until the OD_{600} reached 0.6 - 0.8. Thereafter, the cell cultures were induced with 0.5 mM IPTG and incubated overnight at 18°C.

Cells were pelleted by centrifuging at 5,524 x g for 10 minutes at 4°C; cell lysis was prompted by suspending cell pellets in 50 mM Tris-HCl (pH 8.2) containing 300 mM NaCl, 10 mM imidazole, and 1 mg/mL lysozyme (Sigma). The lysates were centrifuged for 30 minutes at 15,344 x g and loaded directly onto a 1 mL HisTrap FF column. After washing with 15 column volumes of lysis buffer, the His-tagged PMDsc was eluted using 50 mM Tris-HCl (pH 7.5), 300 mM NaCl, and 240 mM imidazole. The eluent proteins were concentrated to 100-500 μM using a Millipore 30,000 MWCO spin column, snap frozen in liquid nitrogen, and stored at -80°C. The activity for wild type PMDsc containing higher salt concentrations was measured to be within error of that found for PMDsc prepared with a desalting step (Kang et al., 2016), which was omitted along with supplementation of purified enzyme with dithiothreitol and glycerol.

4.7 Enzyme characterization and kinetics of PMD

In vitro enzyme kinetics of PMDsc were performed as described in the previous study (Kang et al., 2016). Briefly, enzymatic activity was determined by a spectrophotometric assay quantifying ADP product formation via the pyruvate kinase/lactate dehydrogenase coupled enzyme assay. Assay mixtures were prepared in 150 μL total volume containing 50 mM HEPES-KOH (pH 7.5), 10 mM $MgCl_2$, 400 μM phosphoenolpyruvate, 400 μM NADH, 4 mM ATP, and 25 U of pyruvate kinase/lactate dehydrogenase. The reaction was initiated by enzyme after incubating PMDsc substrate and cofactor for fifteen minutes with coupled assay components. The MVAP was varied from 0.100 - 4.0 mM, and the reaction velocity was determined by monitoring the absorbance at 340 nm in a Spectramax 384plus microplate reader (Molecular Devices, USA). To obtain kinetic data relevant to non-competitive substrate inhibition, MVAP was varied from 0.100 - 100 mM. Enzyme concentration (ε = 56,630 M^{-1} cm^{-1}) was determined spectrophotometrically at 280 nm with a NanoDrop ND-1000 spectrophotometer. k_{cat} and K_M

were derived for PMDsc mutants by fitting the initial velocities measured from 0.100 - 4.0 mM MVAP to the Michaelis-Menten equation; K_I was determined for select mutants by fitting initial velocities measured from 0.100 - 100 mM MVAP to the non-competitive substrate inhibition equation. All kinetic analysis was performed in Graphpad Prism, version 7.0a.

Acknowledgements

This work was part of the DOE Joint BioEnergy Institute (http://www.jbei.org) supported by the U.S. Department of Energy, Office of Science, Office of Biological and Environmental Research, through contract DE-AC02-05CH11231 between Lawrence Berkeley National Laboratory and the U.S. Department of Energy. The United States Government retains and the publisher, by accepting the article for publication, acknowledges that the United States Government retains a non-exclusive, paid-up, irrevocable, world-wide license to publish or reproduce the published form of this manuscript, or allow others to do so, for United States Government purposes.

Reference

Adolfsen, K. J., Brynildsen, M. P., 2015. Futile cycling increases sensitivity toward oxidative stress in Escherichia coli. Metab Eng. 29**,** 26-35.

Atsumi, S., Hanai, T., Liao, J. C., 2008. Non-fermentative pathways for synthesis of branched-chain higher alcohols as biofuels. Nature. 451**,** 86-U13.

Barta, M. L., McWhorter, W. J., Miziorko, H. M., Geisbrecht, B. V., 2012. Structural basis for nucleotide binding and reaction catalysis in mevalonate diphosphate decarboxylase. Biochemistry. 51**,** 5611-21.

Barta, M. L., Skaff, D. A., McWhorter, W. J., Herdendorf, T. J., Miziorko, H. M., Geisbrecht, B. V., 2011. Crystal structures of Staphylococcus epidermidis mevalonate diphosphate decarboxylase bound to inhibitory analogs reveal new insight into substrate binding and catalysis. J Biol Chem. 286**,** 23900-10.

Beller, H. R., Lee, T. S., Katz, L., 2015. Natural products as biofuels and bio-based chemicals: fatty acids and isoprenoids. Nat Prod Rep. 32**,** 1508-26.

Bonanno, J. B., Edo, C., Eswar, N., Pieper, U., Romanowski, M. J., Ilyin, V., Gerchman, S. E., Kycia, H., Studier, F. W., Sali, A., Burley, S. K., 2001. Structural genomics of enzymes involved in sterol/isoprenoid biosynthesis. Proc Natl Acad Sci U S A. 98**,** 12896-901.

Chen, M., Poulter, C. D., 2010. Characterization of thermophilic archaeal isopentenyl phosphate kinases. Biochemistry. 49**,** 207-17.

Chou, H. H., Keasling, J. D., 2012. Synthetic pathway for production of five-carbon alcohols from isopentenyl diphosphate. Applied and environmental microbiology. 78**,** 7849-55.

Cohen, B. E., 2014. Functional linkage between genes that regulate osmotic stress responses and multidrug resistance transporters: challenges and opportunities for antibiotic discovery. Antimicrob Agents Chemother. 58**,** 640-6.

Funke, M., Buchenauer, A., Mokwa, W., Kluge, S., Hein, L., Müller, C., Kensy, F., Büchs, J., 2010. Bioprocess control in microscale: scalable fermentations in disposable and user-friendly microfluidic systems. Microb Cell Fact. 9**,** 86.

George, K. W., Alonso-Gutierrez, J., Keasling, J. D., Lee, T. S., 2015a. Isoprenoid drugs, biofuels, and chemicals--artemisinin, farnesene, and beyond. Adv Biochem Eng Biotechnol. 148**,** 355-89.

George, K. W., Chen, A., Jain, A., Batth, T. S., Baidoo, E. E., Wang, G., Adams, P. D., Petzold, C. J., Keasling, J. D., Lee, T. S., 2014. Correlation analysis of targeted proteins and metabolites to assess and engineer microbial isopentenol production. Biotechnology and bioengineering. 111**,** 1648-58.

George, K. W., Thompson, M. G., Kang, A., Baidoo, E., Wang, G., Chan, L. J., Adams, P. D., Petzold, C. J., Keasling, J. D., Lee, T. S., 2015b. Metabolic engineering for the high-yield production of isoprenoid-based C(5) alcohols in E. coli. Sci Rep. 5**,** 11128.

Gogerty, D. S., Bobik, T. A., 2010. Formation of isobutene from 3-hydroxy-3-methylbutyrate by diphosphomevalonate decarboxylase. Applied and environmental microbiology. 76**,** 8004-10.

Hengge, R., 2008. The two-component network and the general stress sigma factor RpoS (sigma S) in Escherichia coli. Adv Exp Med Biol. 631**,** 40-53.

Heuston, S., Begley, M., Gahan, C. G., Hill, C., 2012. Isoprenoid biosynthesis in bacterial pathogens. Microbiology. 158**,** 1389-401.

Kang, A., George, K. W., Wang, G., Baidoo, E., Keasling, J. D., Lee, T. S., 2016. Isopentenyl diphosphate (IPP)-bypass mevalonate pathways for isopentenol production. Metab Eng. 34**,** 25-35.

Krepkiy, D., Miziorko, H. M., 2004. Identification of active site residues in mevalonate diphosphate decarboxylase: implications for a family of phosphotransferases. Protein Sci. 13**,** 1875-81.

Krepkiy, D. V., Miziorko, H. M., 2005. Investigation of the functional contributions of invariant serine residues in yeast mevalonate diphosphate decarboxylase. Biochemistry. 44**,** 2671-7.

Lange, B. M., Croteau, R., 1999. Isopentenyl diphosphate biosynthesis via a mevalonate-independent pathway: isopentenyl monophosphate kinase catalyzes the terminal enzymatic step. Proc Natl Acad Sci U S A. 96**,** 13714-9.

Lee, T. S., Krupa, R. A., Zhang, F., Hajimorad, M., Holtz, W. J., Prasad, N., Lee, S. K., Keasling, J. D., 2011. BglBrick vectors and datasheets: A synthetic biology platform for gene expression. J Biol Eng. 5**,** 12.

Liu, H. W., Wang, Y., Tang, Q., Kong, W. T., Chung, W. J., Lu, T., 2014. MEP pathway-mediated isopentenol production in metabolically engineered Escherichia coli. Microb Cell Fact. 13.

Mack, J. H., Rapp, V. H., Broeckelmann, M., Lee, T. S., Dibble, R. W., 2014. Investigation of biofuels from microorganism metabolism for use as anti-knock additives. Fuel. 117**,** 939-943.

Martin, V. J., Pitera, D. J., Withers, S. T., Newman, J. D., Keasling, J. D., 2003. Engineering a mevalonate pathway in Escherichia coli for production of terpenoids. Nat Biotechnol. 21**,** 796-802.

Martinez, J. L., Baquero, F., 2000. Mutation frequencies and antibiotic resistance. Antimicrob Agents Chemother. 44**,** 1771-7.

McCullum, E. O., Williams, B. A., Zhang, J., Chaput, J. C., 2010. Random mutagenesis by error-prone PCR. Methods Mol Biol. 634**,** 103-9.

Packer, M. S., Liu, D. R., 2015. Methods for the directed evolution of proteins. Nat Rev Genet. 16**,** 379-94.

Saraste, M., Sibbald, P. R., Wittinghofer, A., 1990. The P-loop--a common motif in ATP- and GTP-binding proteins. Trends Biochem Sci. 15**,** 430-4.

Sun, Y., Fukamachi, T., Saito, H., Kobayashi, H., 2011. ATP requirement for acidic resistance in Escherichia coli. J Bacteriol. 193**,** 3072-7.

Weerasinghe, S., Samantha Dassanayake, R., 2010. Simulation of structural and functional properties of mevalonate diphosphate decarboxylase (MVD). J Mol Model. 16**,** 489-98.

Zhang, B., Watts, K. M., Hodge, D., Kemp, L. M., Hunstad, D. A., Hicks, L. M., Odom, A. R., 2011. A second target of the antimalarial and antibacterial agent fosmidomycin revealed by cellular metabolic profiling. Biochemistry. 50**,** 3570-7.

Table 1 Mutated residues found in 15 replicates of random mutagenesis libraries. All mutations were confirmed by sequencing, and three libraries (L8, L9, L15) included silent mutations. Number of silent mutations refers to number of mutated nucleotides without altering wild type amino acids.

ID	Mutated Residues	Number of silent mutations
L1	Q210H	
L2	R74G, R147K	
L3	Wild type	
L4	Wild type	
L5	V230E	
L6	Q210H	
L7	S186C	
L8	Q140L, I226V	3
L9	R74G, E144D	3
L10	Wild type	
L11	Wild type	
L12	Q210H	
L13	Q210H	
L14	Q210H	
L15	R74G, E144D	4

642 **Table 2** Enzyme kinetics (k_{cat}, K_M and k_{cat}/K_M), growth rates (hr^{-1}) and isopentenol titers (at
643 48 hr, mg/L) of PMDsc mutants. N.D.: not detected. The numbers in brackets are either standard
644 errors (kinetics) or standard deviation (growth rates and titers).

Mutant	**k_{cat}, sec^{-1}**	**K_M, mM**	**k_{cat}/K_M, mM^{-1} sec^{-1}**	**Growth rate, hr^{-1}**	**48hr Titer, mg/L**
WT	0.15 (0.01)	2.3 (0.2)	0.066 (0.007)	0.39 (0.02)	475 (40)
Y19H	0.27 (0.01)	0.35 (0.02)	0.78 (0.06)	0.22 (0.01)	388 (9)
K22Y	0.09 (0.01)	1.3 (0.3)	0.12 (0.03)	0.13 (0.11)	22 (8)
R74G	0.14 (0.02)	3.4 (1.0)	0.04 (0.01)	0.81 (0.03)	975 (96)
R74H	0.33 (0.03)	0.75 (0.05)	0.44 (0.05)	0.68 (0.04)	770 (263)
I145A	0.029 (0.004)	2 (1)	0.01 (0.01)	0.17 (0.00)	623 (140)
R147K	0.149 (0.006)	0.5 (0.1)	0.32 (.09)	0.56 (0.02)	793 (22)
S186C	0.07 (0.01)	0.8 (0.2)	0.08 (0.02)	0.30 (0.02)	596 (110)
M212Q	0.35 (0.02)	0.7 (0.2)	0.5 (0.1)	0.09 (0.01)	601 (76)
I226V	0.16 (0.01)	0.34 (0.06)	0.46 (.09)	0.35 (0.01)	633 (53)
V230E	0.07 (0.01)	0.8 (0.2)	0.08 (0.02)	0.21 (0.18)	278 (91)
R74G-R147K	0.22 (0.01)	0.53 (0.05)	0.42 (0.05)	0.84 (0.04)	909 (25)
R74H-R147K-M212Q	0.16 (0.02)	0.4 (0.2)	0.4 (0.1)	0.79 (0.03)	1079 (27)
R74G-R147K-M212Q	0.22 (0.04)	0.5 (0.1)	0.5 (0.2)	N. D.	8 (1)
R74G-R147K-Q140L	0.06 (0.01)	2(1)	0.03 (0.02)	N. D.	401 (10)

645

646

Table 3 Analysis of Ki and k_{obs} for select mutants. N.D.: not detected.

	k_{cat}, sec^{-1}	K_M, mM	K_i, mM	k_{obs}, sec^{-1}	Growth rate, hr^{-1}	48hr Titer, mg/L
WT	0.15	2.3	18	0.02 (0.01)	0.39 (0.02)	475 (40)
R74G	0.14	3.4	110	0.07 (0.04)	0.81 (0.03)	975 (96)
V230E	0.07	0.8	10	0.006 (0.004)	0.2 (0.2)	278 (91)
R74G-R147K-M212Q	0.22	0.5	11	0.022 (0.008)	N.D.	8 (1)
R74H-R147K-M212Q	0.16	0.43	80	0.07 (0.03)	0.79 (0.03)	1079 (27)

List of Figures

Figure 1 Schematic diagrams of (A) the IPP-bypass isopentenol pathway catalyzed by AtoB, HMGS, HMGR, MK and PMD (solid arrows) and three reactions by PMK, PMD and NudB (dotted arrows) included in the original MVA pathway, and (B) design of the pathways for screening platform, which includes IP kinase (IPK) and IPP isomerase (Idi) in addition to 5 reactions in IPP-bypass isopentenol pathway. Abbreviations: Ac-CoA, acetyl-CoA; AAc-CoA, acetoacetyl-CoA; HMG-CoA, 3-hydroxy-3-methyl-glutaryl-CoA; MVA, mevalonate; MVAP, mevalonate phosphate; MVAPP, mevalonate diphosphate; IPP, isopentenyl diphosphate; IP, isopentenyl monophosphate.

Figure 2 Development and optimization of the screening platform (A) Test of three isopentenyl phosphate (IP) kinases with wild type PMDsc (WT) or S208E mutant: EcIPK, IP kinase from *E. coli*; MtIPK, IP kinase from *Methanothermobacter thermautotrophicus*; Ta IPK, IP kinase from *Thermoplasma acidophilum*. Two concentrations of aTc (10 nM and 100 nM) were used for expression of PMD genes. (B) Test of four PMDsc sequences (WT, K22M, R74H and S208E) with MtIPK. Expression of four PMDsc mutants were induced by 10mM arabinose. Relative growth rate (h^{-1}) and relative activity were on the table. Shaded area is standard error of four biological replicates.

Figure 3 Screening of targeted saturation mutagenesis library (A) Residues for saturation mutagenesis including Tyr19, Lys22, Arg74, Ser208, Thr209 and Met212; MVAP, mevalonate phosphate; ATP, adenosine triphosphate. (B-C) Isopentenol production titers of single mutants (B) and double mutants (C) including R74H, which was previously identified. Light grey bars are titers measured 24 hours after induction and dark grey bars are titers after 48 hours of induction. The reference line is the titer of wild type PMDsc (WT) 48 hours after induction. Titers were calculated with three biological replicates (n = 3).

Figure 4 Screening of random mutagenesis library. (A) Isopentenol titers produced from DH1 strains containing JBEI-9310 (Supplementary Table 1) and various PMDsc mutants concurrently identified from random mutagenesis libraries and (B) single mutant of the identified residue. (C) Triple mutants were generated based on promising residues identified in this study and the previous study (Kang et al., 2016). The reference line at 475.1 mg/L is isopentenol titer of wild type PMDsc (WT) after 48 hours induction and thicker reference line at 1079.1 mg/L is maximum isopentenol titer of the mutant, R74H-M212Q-R147K after 48 hours of induction. Light grey bars are titers after 24 hours induction and dark grey bars are titers after 48 hours of induction. Titers were calculated with three biological replicates (n = 3).

Figure 5 A cartoon representation of PMDsc structure with the 9 identified residues in this study. Four helix secondary structures are highlight with the substrate, MVAP: α-helix 1 (H1, skyblue), α-helix 2 (H2, mustard); α-helix 4 and α-helix 5 (H4-H5, purple).

Figure 6. Isopentenol titers and growth rates of 21 mutants (filled circles) with standard deviation of three biological replicates. Two reference lines (dotted) are wild type's growth rate (0.4) and isopentenol titer (475 mg/L). R^2 and the trend line (solid) were generated by linear regression.

Figure 7 Determination of the noncompetitive substrate inhibition constant, K_I, for select PMDsc mutants: WT (circles); R74G (squares); V230E (upward triangles); R74G:R147K:M212Q (downward triangles); R74H:R147K:M212Q (diamonds). All activities reported are normalized relative to each mutant's k_{cat} derived from fits to the noncompetitive substrate inhibition expression. Parameters were derived from three technical replicates (n = 3).

List of Supplementary Tables and Figures

Supplementary Table S1 List of strains and plasmids

Supplementary Table S2 List of primers to generate mutagenesis

Supplementary Figure S1 Susceptibility test of three *E. coli* strains (BW25113, DH1 and BL21 (DE3)) treated with four different concentration of fosmidomycin (FOS): 0, 10, 50 and 100 nM FOS. Shaded area is standard error of three biological replicates.

Supplementary Figure S2 Test of four PMDsc sequences (WT, K22M, R74H and S208E) with MtIPK. Expression of four PMDsc mutants were induced by (A) 10 nM aTc or (B) 100 nM aTc. Shaded area is standard error of three biological replicates. The included table (C) shows relative growth rate and activity of each PMDsc variants.

Supplementary Figure S3 Chromatogram of 4 nucleotides (A, green; C, blue; G, black; and T, red) detected at the two residues, Lys22 (K22) and Arg74 (R74). Arrow indicates that intensity of nucleotides coding arginine (TCT) decreased residue 74 over time while those of histidine (ATG) increased (Left column), suggesting DH1 with PMDsc R74H has become dominant. One the other hand, nucleotides coding methionine (CAT) at residue 22 was substituted back to wild type lysine (TTT), suggesting that DH1 with expression PMDsc K22M was outcompeted by either wild type or R74H mutants. Intensity of nucleotides at two residues was monitored for three days (Day 1 to Day 3), and codon of four amino acids are written in reverse-complement.

Supplementary Figure S4 Space filling model showing a potential gatekeeper interaction between Arg74 (blue spheres) and a substrate binding loop (green spheres) that shields the active site from bulk solvent.

Supplementary Figure S5 Chromatogram of nucleotides (A, green; C, blue; G, black; and T, red) detected at residue 208 and 209 after the screening. Saturated mutagenesis libraries of two wild type residues, Ser208 and Thr209 were constructed by substituting the residue with NNK.

Arrow indicates positions of randomized nucleotides for Ser208 (CGA) or Thr209 (CGT). Mixed signals of nucleotides at T209 residue (grey arrows) indicates that there was relatively less selection pressure on residue 209 as the mixed nucleotides represents co-existence of various mutants. However, serine clearly dominated at residue 208 (blue arrows; CGA or AGA). N represents all 4 nucleotides and codons of amino acids are written in reverse-complement due to sequencing direction.

Supplementary Figure S6 Cartoon representation of PMDsc with location of essential residues. α-helix 2 (H2, mustard) includes Ser120, Ser121, Ser155 and Arg158 and α-helix 4 (H4, purple) includes Ser208. All serine residues and Arg158 have critical roles in stabilization of substrates including mevalonate diphosphate (MVAP). Grey area is the surface representation of the nearby molecules.

Supplementary Figure S7 Relationship between k_{cat} and cellular growth rates (A); and 48hr isopentenol titers (B) for the characterized PMDsc mutants. Shown in (C) and (D) are the same respective relationships between the observed turnover number, k_{obs}, calculated using non-competitive substrate inhibition at 100 mM MVAP.

735 Figure 1.

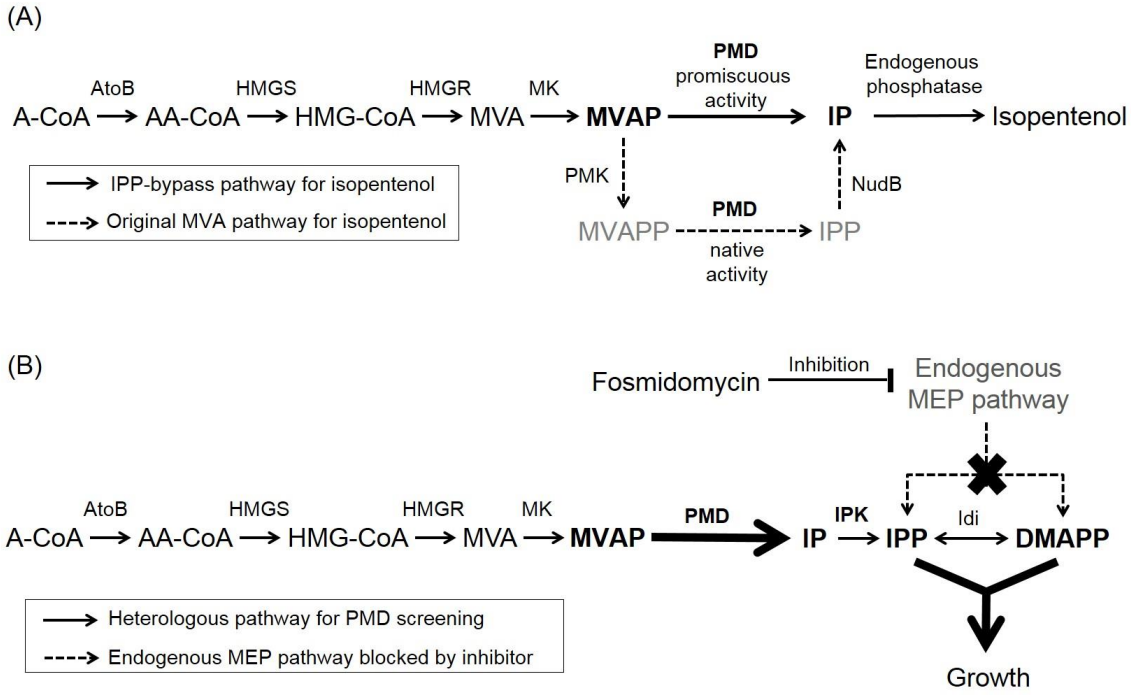

736

737

738 Figure 2

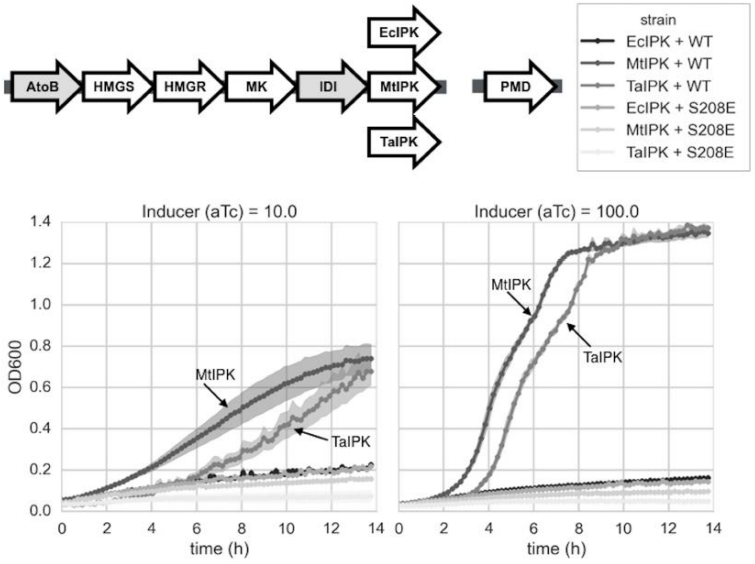

739 Figure 2a

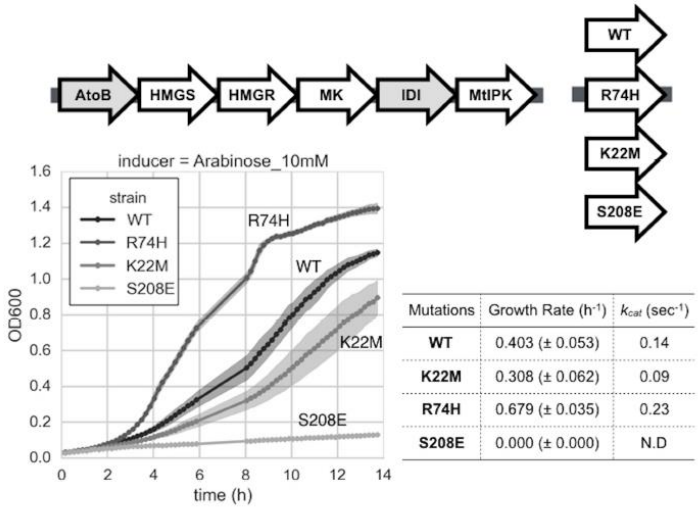

Mutations	Growth Rate (h^{-1})	k_{cat} (sec^{-1})
WT	0.403 (± 0.053)	0.14
K22M	0.308 (± 0.062)	0.09
R74H	0.679 (± 0.035)	0.23
S208E	0.000 (± 0.000)	N.D

740 Figure 2b

741

742 Figure 3

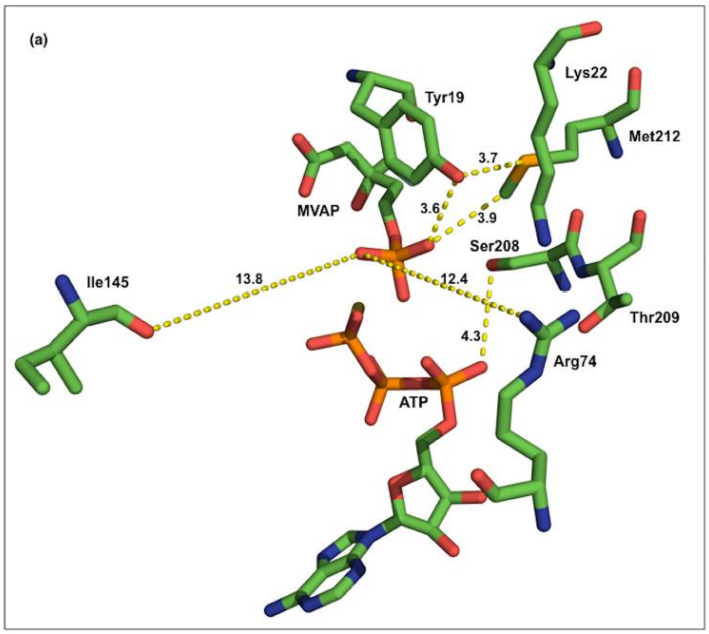

743

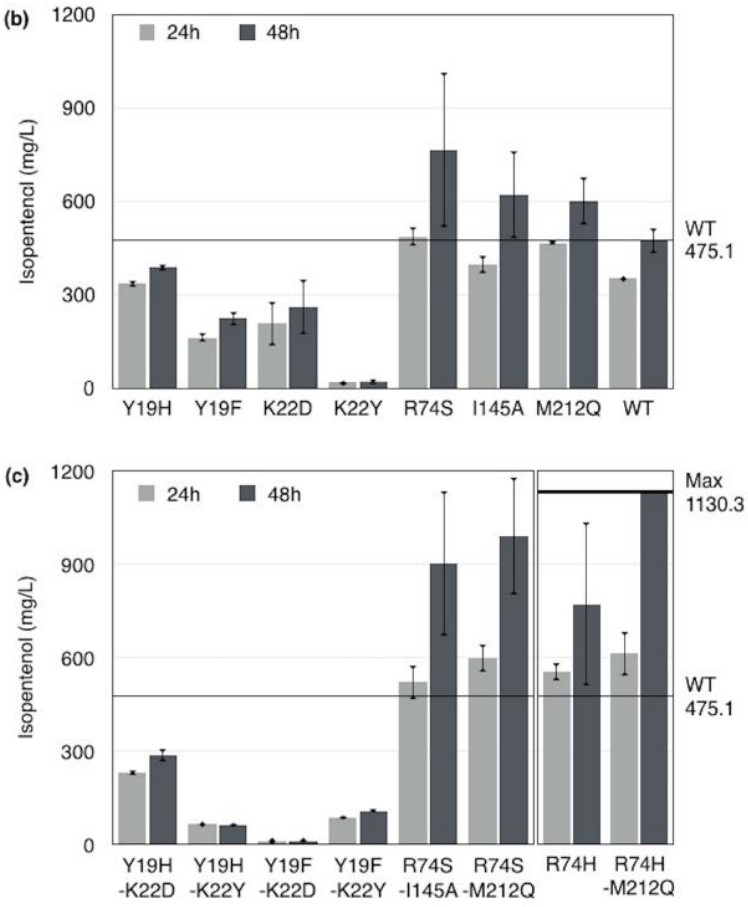

744

745 Figure 4

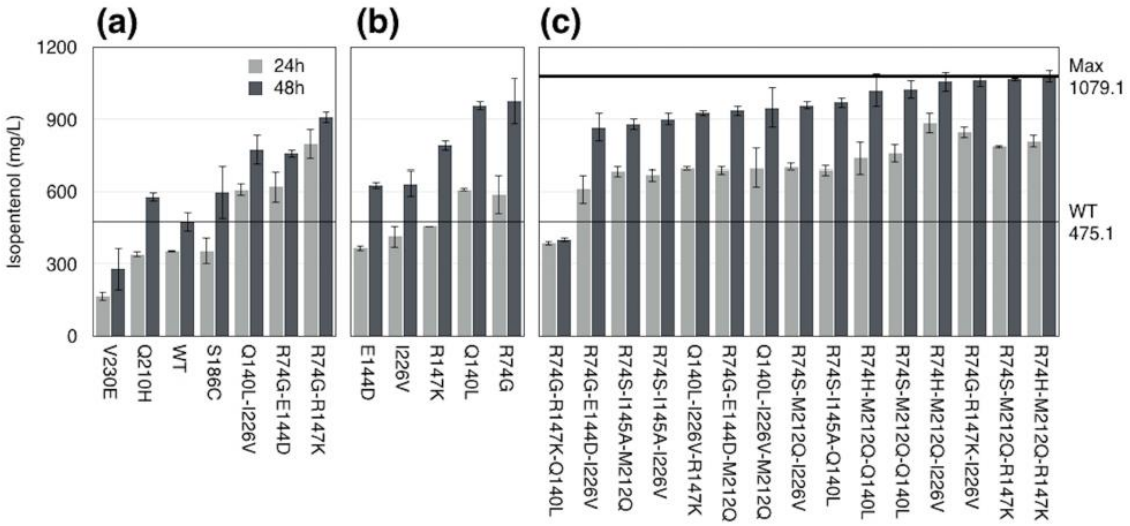

746

747

748 Figure 5

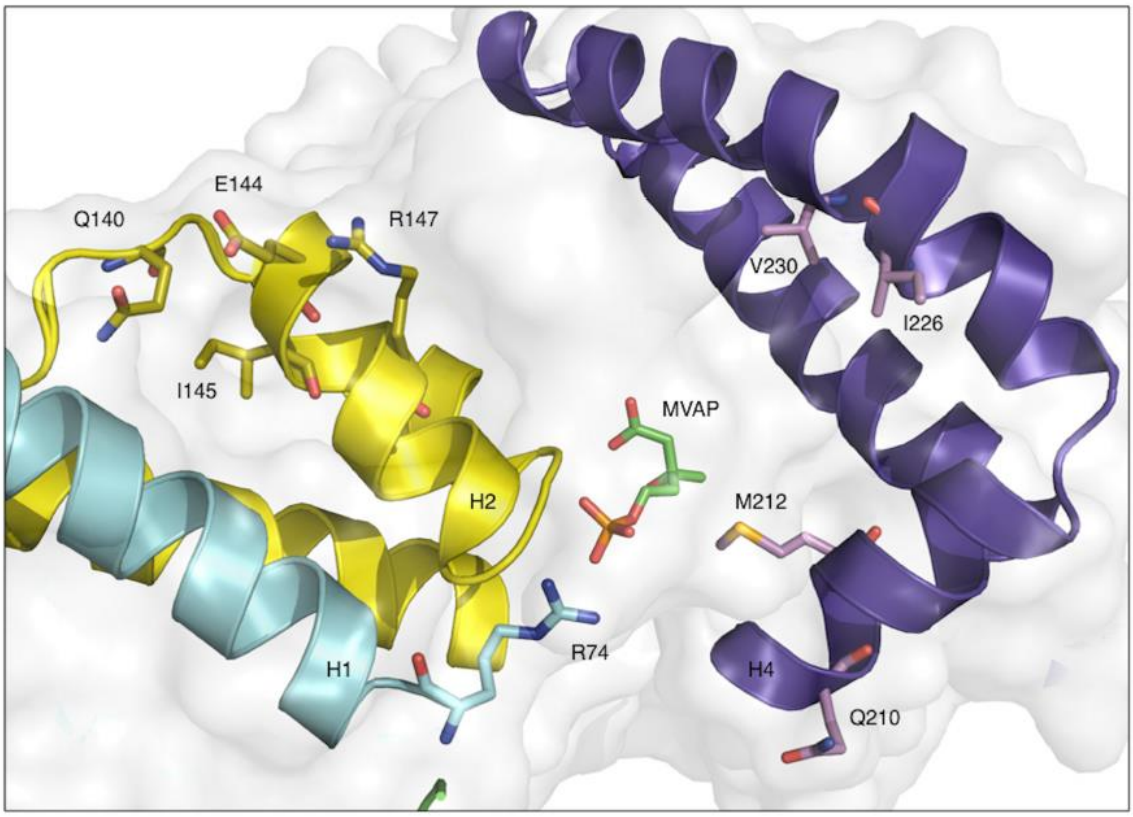

749

750

751 Figure 6

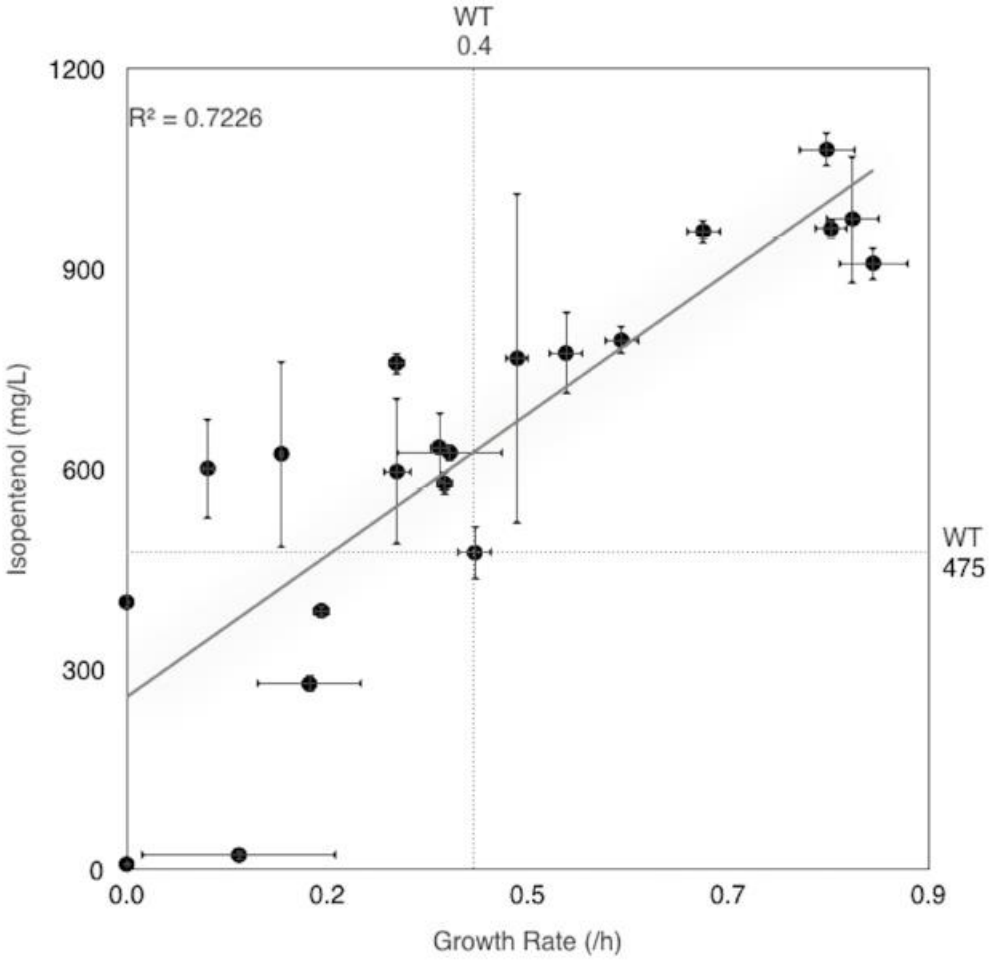

752

753

754 Figure 7

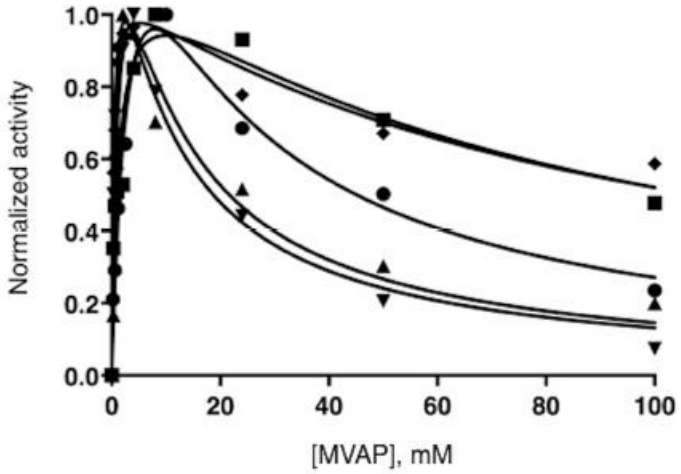

755